Article

Not peer-reviewed version

Adaptive-Step Perturb-and-Observe Algorithm for Multidimensional Phase Noise Stabilization in Fiber-Based Multi-Arm Mach-Zehnder Interferometers

H. Abarzua , C. Melo , S.E. Restrepo , S. Vergara , D. Sbarbaro , G. Cañas , G. Lima , G. Saavedra , J. Cariñe *

Posted Date: 17 October 2024

doi: 10.20944/preprints202410.1296.v1

Keywords: Optical phase noise; Quantum Information; Multi-arm Mach-Zehnder interferometers

Article

Adaptive-step Perturb-and-Observe Algorithm for Multidimensional Phase Noise Stabilization in Fiber-Based Multi-arm Mach-Zehnder Interferometers

H. Abarzúa [1], C. Melo [2], S. E. Restrepo [1,3], S. Vergara [1,3], D. Sbarbaro [2], G. Cañas [4], G. Lima [5], G. Saavedra [2] and J. Cariñe [1,*]

[1] Departamento de Ingeniería Eléctrica, Universidad Católica de la Santísima Concepción, Concepción, Chile
[2] Departamento de Ingeniería Eléctrica, Universidad de Concepción, Concepción, Chile
[3] Centro de Energía, Universidad Católica de la Santísima Concepción, Concepción, Chile
[4] Departamento de Física, Universidad del Bío-Bío, Collao 1202, 5-C Concepción, Chile
[5] Departamento de Física, Universidad de Concepción, Concepción, Chile
* Correspondence: jcarine@ucsc.cl

Abstract: Fiber-optic Mach-Zehnder interferometers are widely used in research areas such as telecommunications, spectroscopy, and quantum information. These optical structures are known to be affected by phase fluctuations that are usually modeled as multiparametric noise.This multidimensional noise must be stabilized or compensated for to enable fiber-optic Mach-Zehnder architectures for practical applications. In this work, we study the effectiveness of a modified Perturb-and-Observe (P&O) algorithm to control multidimensional phase noise in fiber-based multi-arm Mach-Zehnder interferometers. We demonstrate the feasibility of stabilizing multidimensional phase noise by numerical simulations using a simple feedback control scheme and analyze the algorithm's performance for systems up to dimension 8x8. We achieved minimal steady-state errors that guarantee high optical visibility in complex optical systems with $N \times N$ matrices (with $N = [2, 3, 4, 5, 6, 7, 8]$).

Keywords: optical phase noise; quantum information; multi-arm; Mach-Zehnder interferometers

1. Introduction

Fiber-based Mach-Zehnder interferometers (MZIs) are used to detect environmental variations, such as temperature, pressure, and mechanical stress, as well as to increase transmission rates in telecommunication systems [1–3]. They have also interesting applications is in quantum communications. for instance, two-arm MZIs have been used to prepare and measure quantum states encoded by two-dimensional paths (qubits), as well as to evaluate entangled quantum systems [4–6]. For this application, the quality (or fidelity) of the qubit state prepared depends on the physical characteristics of the interferometer, such as polarization, and insertion loss. Although insertion loss and polarization are typically compensated for using passive elements integrated into optical fibers, such as the relative phase between the optical paths changes constantly and randomly due to variations in the refractive index caused mainly by mechanical disturbances and temperature changes.This variation in the optical path between different fibers produces a phase shift that is known as phase noise. To enable quantum information applications, this phase noise has been compensated using various control methods in two-arm MZI, such as piezoelectric and/or fiber stretcher elements, showing successful performance in laboratory and field environments [7–9]. On the other hand, a multi-arm MZI (MAMZI) allows the preparation and measurement of high-dimensional quantum states, known as qudits. One of the most significant advantages of operating with qudits is the ability to encode more information into a single particle compared to a qubit, potentially improving the efficiency of specific quantum tasks, optimizing the execution of quantum algorithms and increasing sensor accuracy across entangled qudits by increasing sensitivity to minor parameter variations [10–12]. In quantum cryptography, qudits offer greater environmental noise tolerance and increased security, as the complexity of eavesdropping attacks grows exponentially with the dimension of the quantum system [13,14].

Although path-encoded qudits can be prepared using a MAMZI, the constant change of the optical path of the multiple arms introduces multidimensional phase noise, making it impractical to

 doi:10.20944/preprints202410.1296.v1

generate and measure qudits efficiently using a single-core fiber array. Multicore optical fibers (MCF) have been employed to mitigate the impact of this phase noise on path-encoded qudits [15–17] and entangled qudits [18]. Although the effects of phase noise are less than in a single-core fiber array, it is still a critical variable in fiber-based MAMZI systems[19]. Quantum cryptography schemes based on MAMZIs have been proposed to: mitigate the impact of multidimensional phase noise by sending the quantum state through all possible paths of the interferometer, thus achieving phase and polarization self-compensation [20]; to implement noise control and encryption process using independent cores of multicore fibers (MCFs)[21], to improve the robustness and quality of the system using hybrid structures such as both single core fibers and MCF within a single MAMZI [22,23].

MAMZIs are composed of multiport beam splitters (MBS), which are feasible to develop directly in multicore fiber [22] and within photonic integrated circuits [20], which allows the scalability of systems of higher complexity ($N > 4$).

In this work we analyze the controllability of any dimensional MAMZI built using MBS. Additionally, we propose a standardized control method that maximizes the specific output intensity of a MAMZI, thus stabilizing the multidimensional phase noise inside the optical circuit. This approach allows optimization algorithms as controllers to mitigate phase noise in any MAMZI configuration. To validate the effectiveness of the proposed method, we use *P&O* algorithm with fixed step sizes [24], evaluating its performance on architectures with $N = [2, 3, 4, 5, 6, 7, 8]$. Adopting a variable step was proposed to improve the fixed step *P&O*. It was tested in photovoltaic systems to improve the speed and accuracy of maximum power point tracking (MPPT) under irradiance variations [25,26]. This variable step approach has been extended to two-arm Mach-Zehnder modulators by adjusting the bias voltage [27]. From this standpoint, in our work, we further revisit the adaptive step scheme in a multi-arm Mach-Zehnder interferometer (MZI), using the intensity error to adjust the step size dynamically, optimizing the system stability under conditions with multiple control parameters, extending *P&O* with adaptive stepping to complex optical systems.

In this way, we verify the effectiveness of the proposed approach by measurement, managing to measure critical parameters such as optical visibility of 0.99 and crosstalk of less than -27dB in $N \times N$ systems, implying that MAMZI systems are suitable for applications in high-dimensional quantum information processing.

2. Multi-Arm Mach-Zehnder Interferometer

A MAMZI is an optical configuration consisting of two MBSs. The first one splits an optical input and guides the resulting beams towards the arms. The optical beams then pass through the arms and are recombined in the second MBS. In this recombination, the optical interference will be affected by the phase information of each arm (ϕ_k^*). A schematic of a MAMZI is shown in Fig. 1.

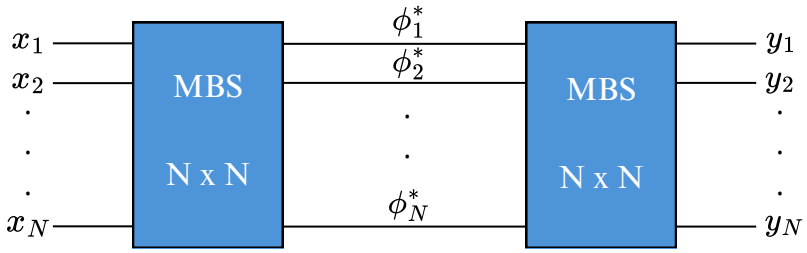

Figure 1. A Multi-Arm Mach-Zehnder Interferometer. x_k and y_k are inputs and outputs respectively. MBS: multi-port beam splitter (N inputs and N outputs). ϕ_k^*: Phase induced in arm k.

The *MBS* can be modelled as a $N \times N$ unitary matrix, with elements $U_{k,l}$ (with $k = [1, ..N]$ and $l = [1..N]$) dependent of a phase $\theta_{k,l}$ induced at each input l related to the k th output, and on the

 doi:10.20944/preprints202410.1296.v1

reflection and optical transmission probabilities of both pairs. A widely used example of ideal MBS is the Fourier matrices described by [28]:

$$F_N = \begin{bmatrix} U_{11} & U_{12}. & ... & U_{1N} \\ U_{21} & U_{22} & ... & U_{2N} \\ \vdots & \vdots & \ddots & \vdots \\ U_{N1} & U_{N2} & ... & U_{NN} \end{bmatrix}, \quad where: \quad U_{k,l} = \frac{1}{\sqrt{N}} e^{\frac{2\pi i(k-1)(l-1)}{N}}. \tag{1}$$

In this case the induced phases are given by $\theta_{k,l} = \frac{2\pi(k-1)(l-1)}{N}$ while the transmission and reflection information is in $\frac{1}{\sqrt{N}}$. On the other hand, considering a MAMZI with attenuations (τ_k) and phases (ϕ_k^*) induced in each arm of the MAMZI, its internal matrix is expressed by:

$$M_N = \begin{bmatrix} \tau_1 e^{i\phi_1^*} & 0 & 0 & 0 \\ 0 & \tau_2 e^{i\phi_2^*} & 0 & 0 \\ \vdots & \vdots & \ddots & \vdots \\ 0 & 0 & \cdots & \tau_N e^{i\phi_N^*} \end{bmatrix}. \tag{2}$$

In our model, τ_k is a complex variable representing the optical loss and polarization changes induced in each arm. Finally, for the MZI architecture, the output optical field (y) can be described as a function of the input optical field (x) using[29]:

$$y = MBS^T \cdot M_N \cdot MBS \cdot x, \tag{3}$$

where the input and output intensities vectors are given by $I^{in} = x^*x$ and $I^{out} = y^*y$, respectively.

3. Fiber optic MAMZI

In a fiber optic MAMZI, the attenuation in each arm (τ_k) can come from the fiber connections, in-line optoelectonic devices, and fabrication defects in the fiber. However, this attenuation is often equalized with external elements, resulting in a common attenuation factor for all arms. Another essential variable is the polarization in the optical fibers, which is omitted in this matrix since commercial polarization controllers can equalize it for all arms [30], allowing the constants τ_k to be considered as unitary values in (2).

To study the controllability of a system consisting of an MBS, we will consider an MBS as:

$$MBS = \frac{1}{\sqrt{N}} \begin{bmatrix} 1 & 1 & ... & 1 \\ 1 & \alpha_{[2,2]} e^{j(\theta_{[2,2]})} & ... & \alpha_{[2,N]} e^{j(\theta_{[2,N]})} \\ \vdots & \vdots & \ddots & \vdots \\ 1 & \alpha_{[N,2]} e^{j(\theta_{[N,2]})} & ... & \alpha_{[N,N]} e^{j(\theta_{[N,N]})} \end{bmatrix}, \tag{4}$$

where $\alpha_{[k,l]}$ and $\theta_{k,l}$ are constant parameters representing attenuation and geometric phases induced in the MBS, respectively. Like the Fourier matrix shown in Eq.(1), the first row, and column contain unit values representing symmetrical splitting ratio and induced phases ($\alpha_{[1,l]} = \alpha_{[k,1]} = 1$ and $\theta_{1,l} = \theta_{k,1} = 0$). The MBS design and manufacturing determine these conditions.

Using the MAMZI model from Eq. (3), the optical intensity at output l for an input $I^{in} = [I_0, 0, ..0]$ is given by:

$$I_l^{out} = \frac{I_0}{N^2} \left\{ \sum_{k=1}^{N} \alpha_{[k,l]}^2 + 2 \sum_{k=1}^{N-1} \sum_{m=k+1}^{N} \alpha_{[k,l]} \alpha_{[m,l]} cos(\theta_{[k,l]} - \theta_{[m,l]} + \phi_{[k]}^* - \phi_{[m]}^*) \right\}. \tag{5}$$

Equation (5) shows how the MAMZI can be processed as a non-linear system, with the internal phase information $\phi_{[k,l]}^*$ as inputs, and the resulting intensity I_l^{out} as outputs, which depends on the

 doi:10.20944/preprints202410.1296.v1

optical interference produced by the phases $\phi^*_{[k,l]}$. To evaluate whether the system is controllable, we must check whether the controllability matrix has full rank [31]. The key term in the expression for I_l^{out} is the sum of cosines whose inputs are the angular differences $(\phi^*_k - \phi^*_m)$. Suppose we have a dynamical system with a state vector $\phi = [\phi^*_1, \phi^*_2, ..., \phi^*_N]$, and with inputs, where each input is $u = \phi^*_k - \phi^*_m$, then incorporating u into equation (5) and partially deriving it we obtain:

$$\frac{dI_l}{du_{[k,m]}} = -\frac{2I_0}{N^2}\left\{\sum_{k=1}^{N-1}\sum_{m=k+1}^{N}\alpha_{[k,l]}\alpha_{[m,l]}sen(\theta_{[k,l]} - \theta_{[m,l]} + u_{[m,k]})\right\} \tag{6}$$

The Jacobian matrix of these partial derivatives will not be zero unless all differences $u_{[k,m]}$ are such that $sin(u_{[k,m]}) = 0$ for all combinations of (k, m). If we consider the space of inputs, as long as there are enough angular variations $u_{[k,m]}$ that make the terms $sin(u_{[k,m]}) = 0$, not all zero simultaneously, the rank of the Jacobian matrix will be complete. Hence, the system will be controllable for the inputs $u_{[k,m]}$.

4. MAMZI with Phase Noise Stabilization

In a MAMZI with phase noise, the phases of the system ϕ^*_k (see equation (2)) are affected by the phase noise ϕ^{noise}_k. To stabilize it, an externally manipulable control phase (ϕ^c_k) will be used, then the phases of the system are modeled as $\phi^*_k = \phi^c_k + \phi^{noise}_k$ with $k \in \{1, 2, ..., N\}$. Note that if it is possible to observe if $\phi^c_k = -\phi^{noise}_k$ (for all k), then M_N converges to the identity matrix. Also, as $MBS^T \cdot I \cdot MBS = I$, then it can be seen that the intensity output from (3) is given by $I^{out} = [I_0.., 0]$. Therefore, it is possible to stabilize a multi-parameter phase noise on an MAMZI by maximizing one of its outputs, which is obtained when a control phase is the negative magnitude of the phase noise applied to each arm. Then, the proposed phase noise stabilization method is obtained from the follow optimization:

$$argmax\{I^{out}_k(\phi^c_k)\} \tag{7}$$

Figure 2 shows the proposed scheme for the phase noise stabilization process. Here, the plant is the MAMZI whose inputs are the information in the internal phases $\phi^*_l = [\phi^*_1, \phi^*_2, ..., \phi^*_N]$, and the outputs are the resulting intensity I^{out}_l, which depends on the optical interference produced by the phases ϕ^*_l. The input optical intensity ($I^{in} I_0$) is a constant.

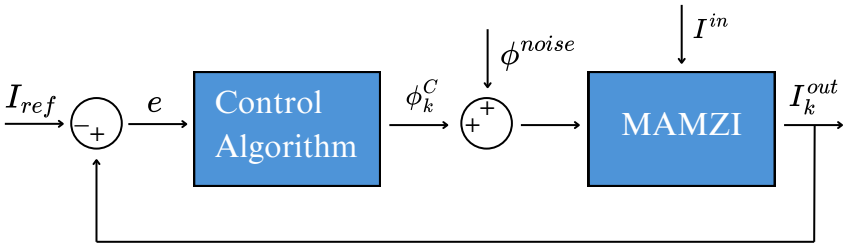

Figure 2. A feedback control scheme for a plant from a MAMZI whose input is the phases and its output is the optical intensity.

In this scheme, the so-called "phase noise" (ϕ^{noise}) is modeled as a disturbance, which is compensated by an actuator of the control system that we call "phase control" (ϕ^C). The controller operates on the error (e) obtained when comparing the output (I^{out}_l) with a reference value (I_{ref}). Note that phases, intensities, errors, and references are vectors of order N.

4.1. MAMZI Simulation with Phase Noise

To evaluate the controllability described above, we have simulated MAMZIs for dimensions 2x2 up to 8x8 using the phased array model, MBSs obtained from the equations Eq. (1), and the phase matrix from Eq. (2). Our simulation is a discrete system, where the phase $\phi^{noise}[n]$ is provided by a matrix of $N \times l_{max} \times M$, where $l_{max} = 40.000$ represents the time length of the simulation, and each

 doi:10.20944/preprints202410.1296.v1

noise sample is a cumulative random sequence with a variability of 0.01π, to mimic the behaviour of fiber MAMZI [22]. We performed $M = 100$ experiments for each simulated control process. The generated phase noise is introduced into the plant "sample by sample," perturbing the intensity equation (5).

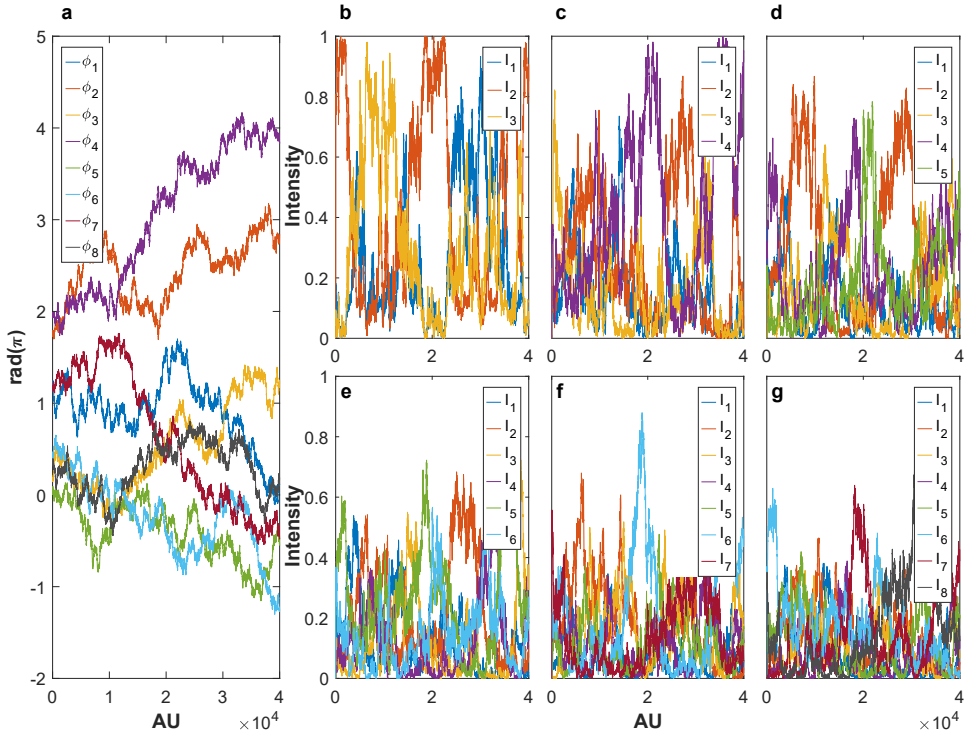

Figure 3. The open loop response. (a) Phase noise matrix used on MAMZI systems. Open loop noise intensity response for: (b) $N = 3$, (c) $N = 4$, (d) $N = 5$, (e)$N = 6$, (f) $N = 7$, and (g) $N = 8$.

Figure 3 shown the open loop intensity response of applied phase noise over diverse MAMZI. Figure 3.a shows one of the 100 matrices of 40.000×8 for the accumulated phase noise simulation, while Figure 3.b-3.g shows the open-loop response of applying N vectors of the noise matrix to the NxN system. Note, for example, that in Figure 3.g, the 8 vectors are used, resulting in a random intensity response for all MAMZI outputs. Each noise matrix was generated, ensuring output intensity with symmetrical temporal distribution.

4.2. Operation of the Control Algorithm

We used an unrestricted direct search algorithm to stabilize the studied system, specifically, *P&O* algorithm, which is recognized for its simplicity and robustness in optimizing systems with multiple degrees of freedom [24]. In MAMZI, the optical intensity of one of the outputs ($I_k^{out}[n]$) will be optimized by perturbing a control phase in each arm ($\phi_k^C[n]$) of the MAMZI as follows:

(i) The algorithm evaluates the error defined as $e[n] = |I_k^{out}[n] - I_{ref}[n]|$, where $I_k^{out}[n]$ is the measured intensity at $k-th$ output and $I_{ref}[n]$ is a reference value. If the error exceeds a predefined threshold (usually less than 0.001 to reach high visibility [22]), the optimization process starts in the initial work cycle ("$wc = 1$").

(ii) As the amplitude of random phase noise in this simulation is 0.01π, the equation perturbs the $wc-th$ phase control as: $\phi_{wc}^C[n] = \phi_{wc}^C[n-1] + 0.01\pi \cdot \delta \cdot sig(\Delta I)$, where the step δ is a manually adjustable value. The sign of the disturbance depends on the variation of $\Delta I = I_k^{out}[n] - I_k^{out}[n-1]$, indicating whether it increases or decreases, reaching a local maximum for $k-th$ output in its phase space.

Preprints.org (www.preprints.org) | NOT PEER-REVIEWED | Posted: 17 October 2024 doi:10.20944/preprints202410.1296.v1

(iii) The algorithm then proceeds to perturb the next phase ("$wc = wc + 1$") of the other arm of the MAMZI, repeating step (ii).
(iv) Once all phases have been processed, the system restarts the cycle from step (i), continuing the iterative optimization process.

4.3. Analysis of the Results in Phase Noise Stabilization

Figure 4 presents the results of applying the *P&O* algorithm to the system with multidimensional noise (for N=2, 4, 6, and 8), according to the scheme shown in Figure 2. Due to the precision in the simulation and to illustrate the system's operation, we show the algorithm *P&O* operating with a value of $\delta = 4$ in each configuration on the complete set of noise matrices described above.

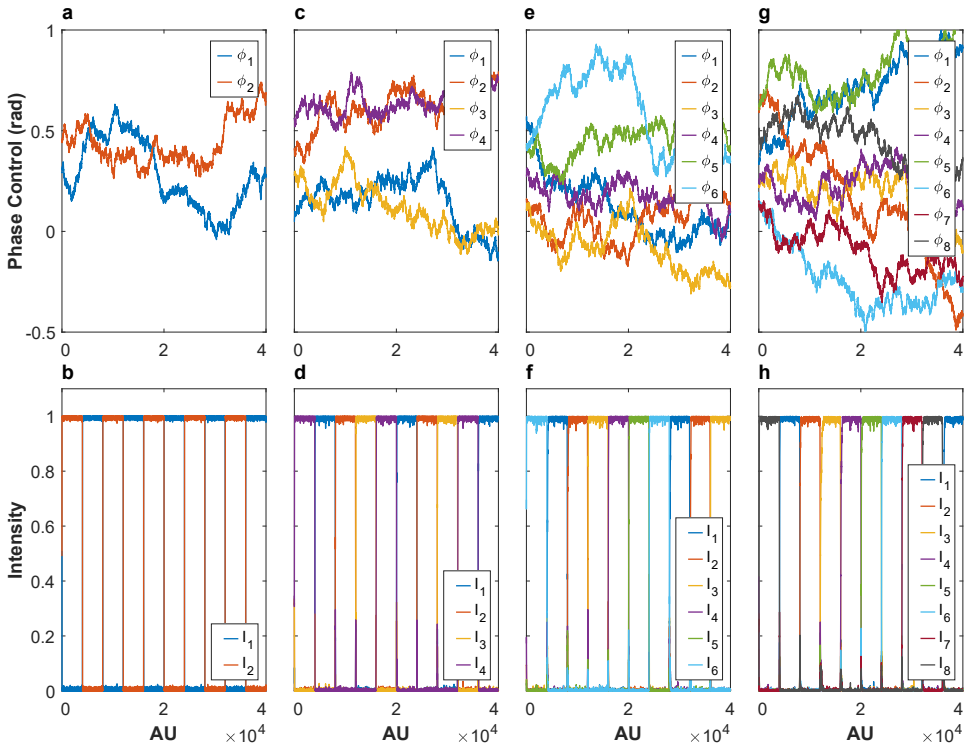

Figure 4. Feedback phase noise control operation. Vertically, a pair of graphs is shown showing the control phases obtained from *P&O* and their respective optical intensity as a function of dimension N, that is: (a) and (b) N=2, (c) and (d) N=4, (e) and (f) N=6, (g) and (h) N=8.

In addition, figure 4 shows the calculated control phases and the respective intensity responses. For example, the results for dimension $N = 2$ are presented in the vertical pair figure 4.a and figure 4.b, while for $N = 4$ they are shown in figure 4.c and figure 4.d, and so on for higher dimensions. The system control operates on each output sequentially, remaining controlled for $\tau_{control} = 4000$, generating ten temporary operation cycles ($\tau_{control} = l_{max}/10$), effectively keeping the outputs maximized and operating the changes at high speed. However, the signals in steady-state show some variability.

 doi:10.20944/preprints202410.1296.v1

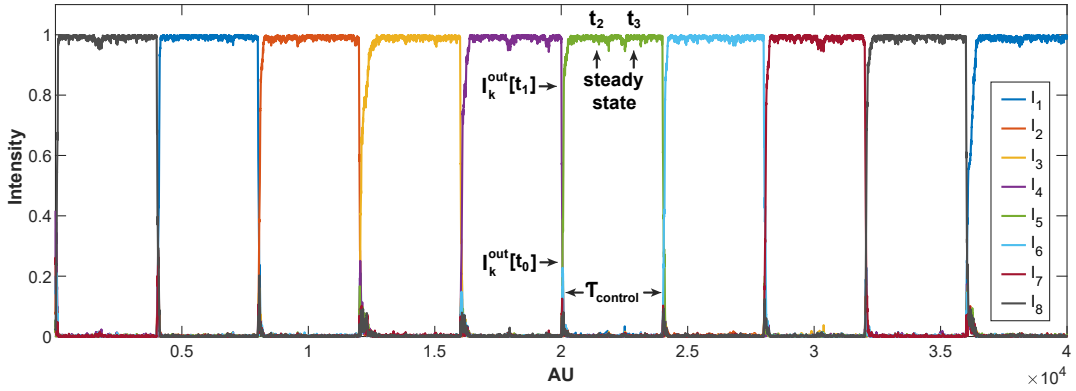

Figure 5. Time labels for calculating control parameters in a stabilized MAMZI for $N = 8$.

Figure 5 shows the system's response of a MAMZI for $N = 8$ under feedback control, using the abovementioned parameters. In this figure, the steady-state variability and the operating speed differences throughout each work cycle can be seen more clearly. In our analysis of the control operation, we used the following four indicators to evaluate the performance of the proposed control method:

Control velocity: evaluates the speed at which the algorithm reaches its maximum intensity, equivalent to stabilizing the phase noise. Therefore, the time taken by the stabilized signal intensity to go from 10% ($I_k^{out}[t_0] = 0.1$) to 90% ($I_k^{out}[t_1] = 0.9$) is measured, as we show in the Figure 5. It is important to note that the sampling period is an arbitrary variable, so the control speed (cv) is given by:

$$cv = \frac{0.8}{t_1 - t_0}. \tag{8}$$

Root Mean Square Error: quantifies the steady-state control error on the stabilized signal. Since the stabilization cycle is $\tau_{control}$, the signal is assumed to reach the steady state from time $t_2 = \tau_{control}/3$. The upper limit is set at time $t_3 = 2\tau_{control}/3$ to obtain a robust statistic (see Figure 5). The $RMSE$ calculation is performed considering this time interval, being estimated from:

$$RMSE = \sqrt{\frac{1}{N_L}\sum_{n=t_2}^{t_3}(I_k^{out}[n] - I_{ref}[n])^2}, \tag{9}$$

where N_L is the total number of points sampled betweeen t_2 and t_3.

Visibility: quantifies the optical interference characteristics of a communications channel. It is especially crucial in quantum systems, where the visibility of the system directly influences the fidelity of quantum state preparation and measurement. Visibility is defined by:

$$V = \frac{I_k^{out}max - I_k^{out}min}{I_k^{out}max + I_k^{out}min}, \tag{10}$$

where $I_k^{out}max$ and $I_k^{out}min$ correspond to maximum and minimum value of I_k^{out} respectively.

Crosstalk: measures the ratio of unwanted information (I_p^{out}) from an external channel to the information that this channel can transmit (I_k^{out}) with $p \neq k$, mathematically it is expressed as:

$$Cr = 10log(\frac{I_p^{out}}{I_k^{out}}) \tag{11}$$

Figure 6 shows the results obtained for the $P\&O$ algorithm using a fixed step considering $1 < \delta < 20$. It is observed that the RMSE remains below 1% for systems smaller than N=6, while for larger N the error does not exceed 2% with $\delta = 3$. Values for δ lower than three were discarded since they

 doi:10.20944/preprints202410.1296.v1

caused the system to lose controllability. Furthermore, an increase in δ accelerates the control system's response, although it increases the error, indicating a less precise operation. This same trend is reflected in the visibility and crosstalk graphs, where it can be seen that, for minimum values for δ the system shows less contamination by crosstalk and greater visibility of interference. However, by increasing δ, the control system works faster when seeking system stabilization, at the cost of more significant crosstalk contamination and a loss in visibility quality.

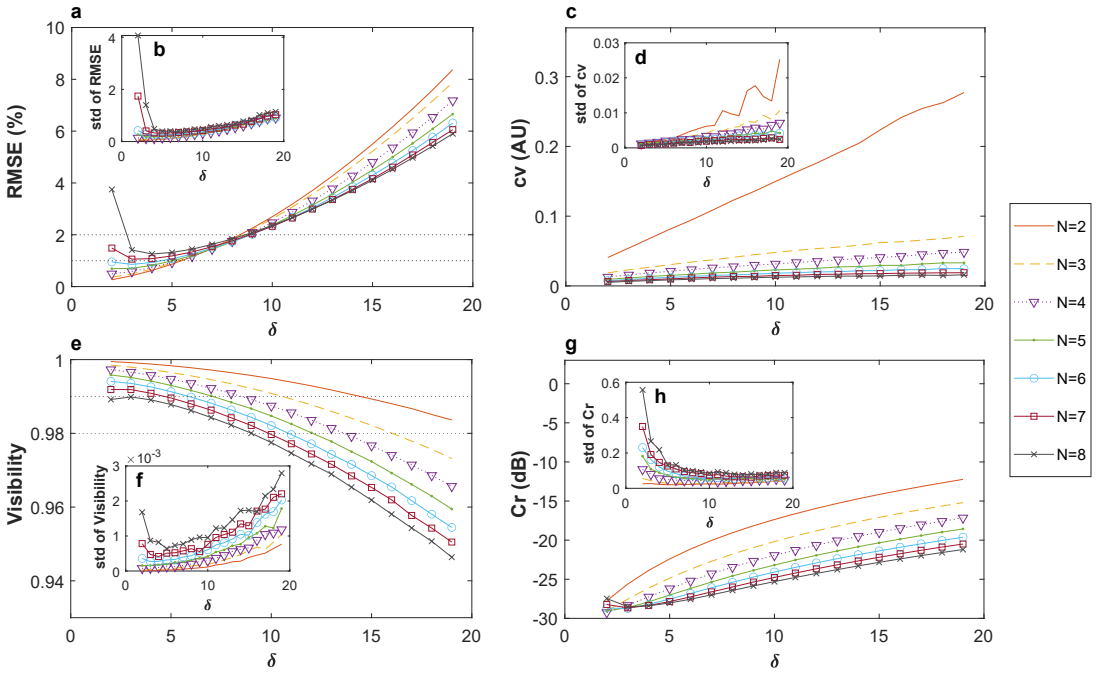

Figure 6. (a) RMSE for orders $N = 2, 3, 4, 5, 6, 7$, and 8. (b) Standard deviation of RMSE for the range $1 < \delta < 20$ using P&O algorithm. (c) Control velocity cv for orders $N = 2$ to $N = 8$. (d) Deviation of cv for $1 < \delta < 20$. (e) Visibility for orders $N = 2$ to $N = 8$. (f) Variation of visibility within $1 < \delta < 20$. (g) Cr parameter for orders $N = 2$ to $N = 8$. (h) Standard deviation of Cr over the interval $1 < \delta < 20$.

Based on the above, improving the system's performance is possible by adapting the step (δ) to increase when more speed is required and reduce when greater precision is needed. To implement this adaptive control, it is proposed that the step be proportional to the error, i.e., $\delta[n] = e[n] \cdot A + \delta_{min}$, where A is a system parameter that regulates the impact of the signal $e[n]$ on the value $\delta[n]$, according to previous results, $\delta_{min} = 3$.

Figure 7 compares the mean and standard deviation values of RMSE and cv as a function of N and A, using the proposed adaptive control. It is observed that both the RMSE and its standard deviation decrease as A increases for systems with $N > 4$. On the other hand, for systems with $N \leq 4$, the improvements are minimal. Furthermore, the speed and its standard deviation increase with A, and, as expected, less complex systems (fewer arms) perform better in terms of RMSE and speed.

Preprints.org (www.preprints.org) | NOT PEER-REVIEWED | Posted: 17 October 2024 doi:10.20944/preprints202410.1296.v1

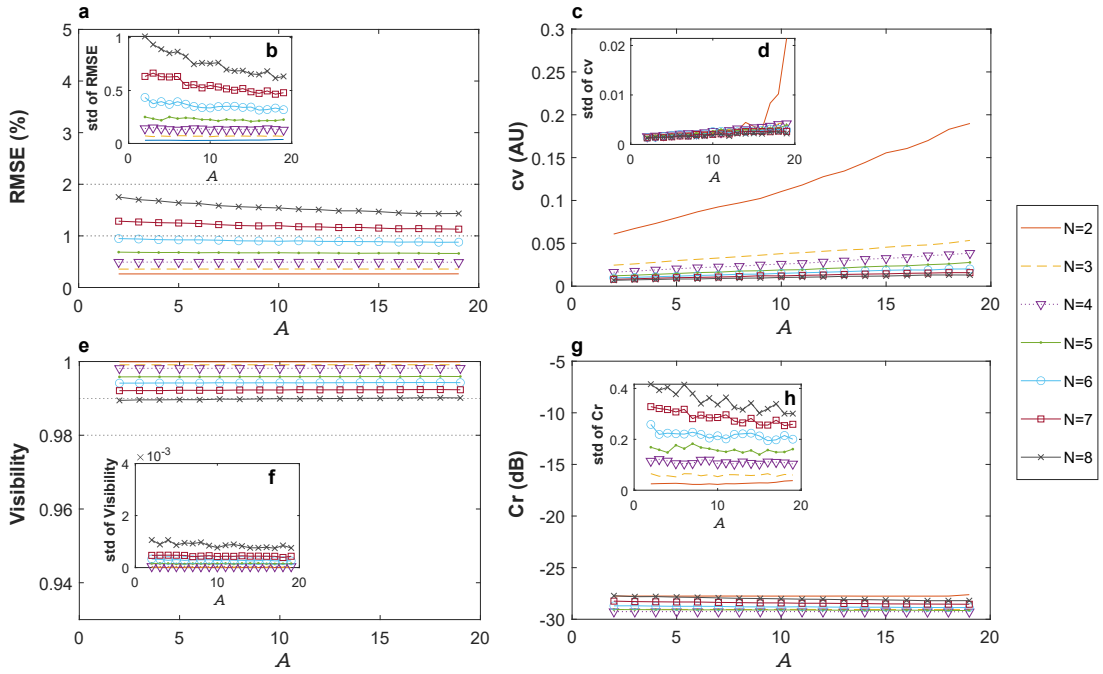

Figure 7. (a) RMSE for orders $N = 2, 3, 4, 5, 6, 7$, and 8. (b) Standard deviation of RMSE. (c) Control parameter cv. (d) Standard deviation of cv. (e) Visibility, which remains practically constant for $N \leq 5$ regardless of A. (f) Standard deviation of visibility. (g) Cr parameter. (h) Standard deviation of Cr.

Regarding visibility, it is observed that adaptive control maintains practically constant values, regardless of A, for systems with $N \leq 5$. For systems with a more significant number of arms ($N > 5$), an increase in visibility is observed, accompanied by a decrease in its standard deviation as A increases (Figure 7). It is relevant to note that almost all visibility values exceed 0.99.

The application of adaptive control maintains practically constant values of visibility, regardless of the increase in speed for all the systems studied, and a decrease in its standard deviation is observed as A increases (Figure 7), which implies that the system is more stable despite being accelerated. It is relevant to highlight that almost all visibility values exceed 0.99. Similarly to visibility, crosstalk shows a mean value that tends to remain constant for all values of N as A increases, following a similar trend in its standard deviation. In addition, it presents lower values concerning $P\&O$ with fixed steps, reflecting a clear improvement in the control process.

In summary, the results obtained by the adaptive steps show that the steady-state error remains below 1% for systems with $N < 5$ and below 2% for higher-order systems, even with higher A. This behavior directly influences the optical parameters, with visibility remaining above 0.99 and crosstalk below $-27dB$ in all cases analyzed, regardless of the system order.

5. Conclusions

In this work, we evaluated the controllability of a MAMZI when it is affected by phase noise. The controllability is demonstrated mathematically based on an essential criterion, and then the control model is used in a numerical emulation, demonstrating the controllability of this system from 2x2 to 8x8. Minor modifications (adaptive steps) in numerical processing can improve the quality indicators in control, such as the steady-state error and control velocity, implying that these results can be improved by applying more advanced algorithms and controllers. Under an optical analysis, the results demonstrate a high-quality interference in the MAMZI at low crosstalk. Our study indicates that any MAMZI under multi-parameter phase noise can be used for high-dimensional quantum information protocols.

Author Contributions: All authors contributed equally to this work.

Acknowledgments: This work was supported by Fondo Nacional de Desarrollo Científico y Tecnológico (ANID) (Grants No. 1240843, 1231826, 1230796, 1240746, ID22I10262), ANID – Millennium Science Initiative Program–ICN17012, Ingeniería 2030 (ING222010004) and InES Ciencia Abierta (INCA210005).

References

1. Elsherif, M., Salih, A.E., Muñoz, M.G., et al , Optical Fiber Sensors: Working Principle, Applications, and Limitations. Adv. Photonics Res., **3**, 2699-9293 (2022)
2. Lecheng Li, Li Xia, Zhenhai Xie, and Deming Liu, "All-fiber Mach-Zehnder interferometers for sensing applications," Opt. Express.**20**, 11109-11120 (2012)
3. Tetsuya K, Takahide S, Tetsuya M, et al, "High-speed optical DQPSK and FSK modulation using integrated Mach-Zehnder interferometers," Opt. Express 14, 4469-4478 (2006)
4. N. Gisin, G. Ribordy, W. Tittel, and H. Zbinden, "Quantum Cryptography", Rev. Mod. Phys. **74**, 145 (2002).
5. A. Cuevas, G. Carvacho, G. Saavedra, et al.,"Long-distance distribution of genuine energy-time entanglement," Nat. Commun **4**, 2871 (2013).
6. F. Vedovato, C. Agnesi, M. Tomasin, M. Avesani, L. Jan-Åke, G. Vallone, and P. Villoresi, "Postselection-Loophole-Free Bell Violation with Genuine Time-Bin Entanglement", Phys. Rev. Lett. **121**, 190401 (2018).
7. D. Grassani, M. Galli, D. Bajoni, "Active stabilization of a Michelson interferometer at an arbitrary phase with subnanometer resolution", Opt. Lett., **39**, 2530-2533 (2014).
8. G. B. Xavier and J. P. V. der Weid, "Stable single-photon interference in a 1 km fiber-optic Mach–Zehnder interferometer with continuous phase adjustment", Opt. Lett. **36**, 1764 (2011).
9. G Carvacho, J. Cariñe, G. Saavedra, et al., "Postselection-Loophole-Free Bell Test Over an Installed Optical Fiber Network", Phys. Rev. Lett. **115**, 030503 – Published 14 July 2015
10. V. Giovannetti, S. Lloyd, and L. Maccone, "Quantum-enhanced measurements: beating the standard quantum limit", Science, **306**, 1330-1336, 2004.
11. M. A. Nielsen and I. L. Chuang, "Quantum Computation and Quantum Information: 10th Anniversary Edition"., Cambridge: Cambridge University Press. 2010.
12. B. P. Lanyon et al., "Simplifying quantum logic using higher-dimensional Hilbert spaces", Nature Physics, **5**, pp. 134-140, 2009.
13. N. J. Cerf, M. Bourennane, A. Karlsson, and N. Gisin, "Security of quantum key distribution using d-level systems", Phys. Rev. Lett. **88**, 127902 (2002).
14. V. Scarani et al., "The security of practical quantum key distribution", Reviews of Modern Physics, **81**, pp. 1301-1350, 2009.
15. G. Cañas, N. Vera, J. Cariñe, et al., "High-dimensional decoy-state quantum key distribution over multicore telecommunication fibers", Phys. Rev. A **96**, 022317 (2017).
16. Ding, Y., Bacco, D., Dalgaard, K. et al. High-dimensional quantum key distribution based on multicore fiber using silicon photonic integrated circuits. npj Quantum Inf, **3**, 25 (2017).
17. Lee, H.J., Choi, SK. and Park, H.S. Experimental Demonstration of Four-Dimensional Photonic Spatial Entanglement between Multi-core Optical Fibres. Sci Rep, **7**, 4302 (2017).
18. E.S. Gómez, S. Gómez, I. Machuca, et al., "Multidimensional Entanglement Generation with Multicore Optical Fibers", Phys. Rev. Applied, **15**, 034024, (2021).
19. L. Gan, R. Wang, D. Liu, L. Duan, S. Liu, S. Fu, B. Li, Z. Feng, H. Wei, W. Tong, et al., "Spatial-division multiplexed Mach–Zehnder interferometers in heterogeneous multicore fiber for multidimensional measurement", IEEE Photonics J. **8**, 7800908 (2016).
20. D. Balado, J. Liñares, X. Prieto-Blanco, and D. Barral, "Phase and polarization autocompensating N-dimensional quantum cryptography in multicore optical fibers," J. Opt. Soc. Am. B, **36**, 2793-2803 (2019).
21. Da Lio, B., Cozzolino, D., Biagi, N. et al. Path-encoded high-dimensional quantum communication over a 2-km multicore fiber. npj Quantum Inf,**7**, 63 (2021).
22. J. Cariñe, G. Cañas, P. Skrzypczyk, et al., "Multi-core fiber integrated multi-port beam splitters for quantum information processing", Optica,**7**, 542-550, 2020.
23. M.M. Taddei, J. Cariñe, D. Martínez, et al., "Computational advantage from the quantum superposition of multiple temporal orders of photonic gates", PRX Quantum,**2**,010320, (2021).

 doi:10.20944/preprints202410.1296.v1

24. Yatinkumar, P. "A Comprehensive Review of Maximum Power Point Tracking Techniques for Photovoltaic Systems". Renewable and Sustainable Energy Reviews, **112**, 379-387. (2020)
25. M. A. Elgendy, B. Zahawi and D. J. Atkinson, "Assessment of Perturb and Observe MPPT Algorithm Implementation Techniques for PV Pumping Applications," IEEE Transactions on Sustainable Energy,**3**, 21-33, (2012)
26. T. Esram and P. L. Chapman, "Comparison of Photovoltaic Array Maximum Power Point Tracking Techniques," in IEEE Transactions on Energy Conversion, **22**, 439-449,(2007).
27. Y. Ji, B. Wu, Y. Hou and A. Ding, "A MZ Modulator Bias Control System Based on Variable Step P&O Algorithm", IEEE Photonics Technology Letters, **32**, 1473-1476,(2020).
28. K Mattle, M Michler, H Weinfurter, A Zeilinger, M Zukowski, "Nonclassical statistics at multiport beamsplitters", Applied Physics B-Lasers and Optics, **60**, 111-117, (1995)
29. G.Weihs, M. Reck, H.Weinfurter, and A. Zeilinger, “All-fiber three-path mach-zehnder interferometer," Opt. Lett., **21**, 302-304, (1996).
30. Thorlabs, Inc. Available at: https://www.thorlabs.com/ (Accessed: 01 October 2024).
31. Preumont, A. "Controllability and Observability", Vibration Control of Active Structures. Solid Mechanics and Its Applications, **179**, 275-297. Springer, (2011).